Pergamon

Geochimica et Cosmochimica Acta, Vol. 65, No. 5, pp. 705–714, 2001

0016-7037/01 $20.00 + .00

PII S0016-7037(00)00611-6

Kinetics of oxygen exchange between sites in the $GaO_4Al_{12}(OH)_{24}(H_2O)_{12}^{7+}$(aq) molecule and aqueous solution

WILLIAM H. CASEY[1,3,*] and BRIAN L. PHILLIPS[2]

[1]Department of Land, Air, and Water Resources, University of California, Davis, CA 95616, USA
[2]Department of Chemical Engineering and Materials Science, University of California, Davis, CA 95616, USA
[3]Department of Geology, University of California, Davis, CA 95616, USA

(*Received July* 5, 2000; *accepted in revised form November* 6, 2000)

Abstract—Rates of steady exchange of oxygens between bulk solution and sites in the $GaO_4Al_{12}(OH)_{24}(H_2O)_{12}^{7+}$(aq) ($GaAl_{12}$) aqueous complex were determined over the temperature range of 301 to 317 K and $4.1 < pH < 4.9$ using ^{17}O–nuclear magnetic resonance (NMR). The $GaAl_{12}$ molecule, like the $AlO_4Al_{12}(OH)_{24}(H_2O)_{12}^{7+}$(aq) ($Al_{13}$) molecule studied previously, has 12 equivalent bonded water molecules (η^1-OH_2 sites), two structurally distinct sets of 12 hydroxyl bridges (μ_2-OH; μ_2-OH′ sites), and four four-coordinated oxo groups (μ_4-O sites).

The $GaAl_{12}$ molecule is much less reactive than the Al_{13} molecule, and this decreased reactivity is not associated with any clear changes in the structural chemistry at the sites of exchange. The rate coefficients for exchange of the water molecules bonded to the complex with bulk water are as follows: $k_{ex}^{298} = 227(\pm 40)\ s^{-1}$, $\Delta H^{\ddagger} = 63(\pm 7)$ kJ mol^{-1}, and $\Delta S^{\ddagger} = 13(\pm 21)$ J mol^{-1} K^{-1}. The rate at 298 K is ≈5 times slower than the corresponding exchange reaction on the Al_{13} molecule, but it falls within the range measured for dissolved aluminum monomers. These data support our earlier speculation that rates of exchange of η^1-OH_2 sites at fully charged aluminum (hydr)oxide mineral surfaces are similar to rates for aqueous aluminum complexes in acids.

The rates of isotopic exchange of the two hydroxyl bridges in the $GaAl_{12}$ complex differ from one another, as we also observed for the Al_{13} complex, but to a much smaller extent. Likewise, the activation parameters for exchange at the two sites are much more similar to one another in the $GaAl_{12}$ molecule than in the Al_{13}. The rate coefficients for exchange of the more reactive hydroxyl bridge are as follows: $k_{ex}^{298} = 1.8(\pm 0.1) \cdot 10^{-5}\ s^{-1}$, $\Delta H_1^{\ddagger} = 98(\pm 3)$ kJ mol^{-1}, $\Delta S_1^{\ddagger} = -8(\pm 9)$ J mol^{-1} K^{-1}, and for the less labile bridge, they are $k_{ex}^{298} = 4.1(\pm 0.2) \cdot 10^{-7}\ s^{-1}$, with $\Delta H_2^{\ddagger} = 125(\pm 4)$ kJ mol^{-1} and $\Delta S_2^{\ddagger} = 54(\pm 12)$ J mol^{-1} K^{-1}. There is no strong pH dependence to rates. *Copyright © 2001 Elsevier Science Ltd*

1. INTRODUCTION

We are attempting to characterize the rates of some geochemically useful molecular reactions and recently reported rate coefficients for steady exchange of oxygens in the $AlO_4Al_{12}(OH)_{24}(H_2O)_{12}^{7+}$(aq) complex ($Al_{13}$) with bulk solution (Casey et al., 2000; Phillips et al., 2000). This structure, which resembles a ε-Keggin molecule (Fig. 1), shares important structural features with mineral surfaces. The molecule polymerizes in solution to form larger polyoxocomplexes (e.g., Fu et al., 1991; Allouche et al., 2000; Rowsell and Nazar, 2000; see also Michot et al., 2000) and ultimately forms amorphous aluminum (hydr)oxide solids that recrystallize to bayerite (Bradley et al., 1993). Through the efforts of several research groups (e.g., Johansson, 1960, 1962a,b; Johansson et al., 1960; Bradley et al., 1990, 1993; Furrer et al., 1992a,b, 1999; Amirbahman et al., 2000), we know much about the aqueous chemistry of this molecule and can employ it as a model for aluminum–(hydr)oxide mineral surfaces.

In this article, we extend our earlier work on the Al_{13} complex to report the rates of oxygen exchanges in the $GaO_4Al_{12}(OH)_{24}(H_2O)_{12}^{7+}$(aq) ($GaAl_{12}$) molecule, which differs from Al_{13} by a single substitution of Ga(III) for Al(III) in the central tetrahedral site (see Bradley et al., 1992). Here we show that this single-atom substitution, which is three bonds away from the exchanging oxygens, has surprisingly large effects on the rates. These effects cannot simply be explained by differences in structure of the $GaAl_{12}$ and Al_{13} molecules in crystals.

*Author to whom correspondence should be addressed (whcasey@ucdavis.edu).

2. MATERIALS AND METHODS

2.1. Crystalline Solids and Preparation of Solutions

We synthesized pure crystals of $Na[GaO_4Al_{12}(OH)_{24}(H_2O)_{12}(SeO_4)_4](H_2O)_x$ by titrating an $AlCl_3$ solution with $NaOH+GaCl_3$ at 85°C. After precipitation, the solutions were cooled and diluted with deionized water, followed by addition of an excess of Na_2SeO_4 to induce crystallization (see Furrer et al., 1992b). The solutions were frequently filtered (0.2 μm) to remove any aluminum- or gallium-hydroxide colloids. After several days, the crystals were sieved under the mother liquor, distilled water, and then methanol to separate 25- to 75-μm-sized crystals.

The identity of the crystalline product was determined by nuclear magnetic resonance (NMR) and by comparing the X-ray structure of a single $Na[GaO_4Al_{12}(OH)_{24}(H_2O)_{12}(SeO_4)_4](H_2O)_x$ crystal with the results of Parker et al. (1997). The crystals were then examined with ^{27}Al-NMR to determine the amount of Al_{13} impurities. These spectra are shown in Figure 2 and indicate that the $GaAl_{12}$ crystals contain ≈0.3% of the aluminum as Al_{13} impurities.

Quantitative solution-state ^{71}Ga-NMR was employed to confirm that the gallium occurs primarily in the tetrahedral site of the $GaAl_{12}$ molecule and does not substitute appreciably for aluminum in the octahedral sites. To accomplish this analysis, we prepared a monospecific solution of $GaAl_{12}$ by dissolving crystals with an $H_2O+BaCl_2$ solution (see Bradley et al., 1992), followed by filtering the solution

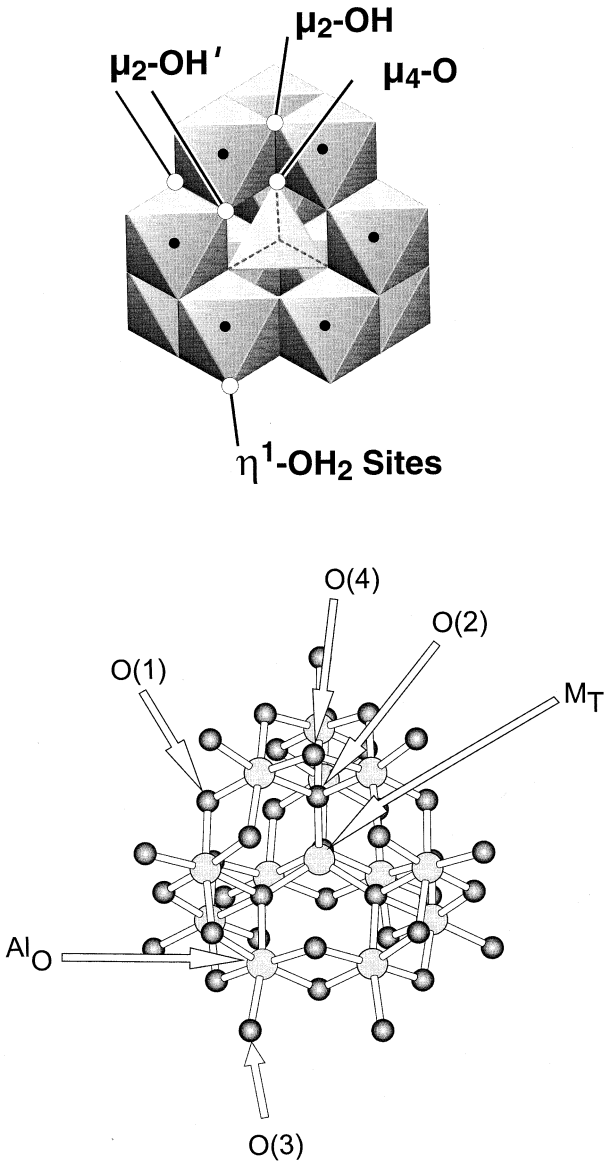

Fig. 1. (Top) Polyhedral representation of the $GaO_4Al_{12}(OH)_{24}(H_2O)_{12}^{7+}$(aq) complex ($GaAl_{12}$), which has a tetrahedral $Ga(O)_4$ unit surrounded by 12 $Al(O)_6$ octahedra. There are 12 equivalent η^1-OH_2 sites and two distinct sets of 12 μ_2-OH at the shared edges of AlO_6 octahedra. These two sets differ in their positions relative to the μ_4-O groups. One site, labeled μ_2-OH′, lies *cis* two μ_4-O groups. The other site, labeled μ_2-OH, lies *cis* to one μ_4-O site. (Bottom) A ball-and-stick representation of the $GaAl_{12}$ structure with the atoms given crystallographic labels (consistent with Parker et al., 1997).

(0.2 μm) into an NMR sample tube. An internal coaxial sample of 0.096 mol/L $Ga(OH)_4^-$(aq) was included to provide a peak in the spectrum of constant intensity at 223 ppm. The intensity of the ^{71}Ga-NMR peak corresponding to the $^{IV}Ga(O)_4$ in the dissolved $GaAl_{12}$ complex (138 ppm) could then be compared with the intensity of the Ga^{3+}(aq) peak (0 ppm) formed by subsequent digestion of the molecule in acid. For an ideal $GaAl_{12}$ stoichiometry, the intensity of the peak corresponding to the $^{IV}Ga(O)_4$ should equal the intensity of the peak at 0 ppm after acidification. We measured a ratio of intensities for these peaks of 1.03($\pm$0.09; $n = 3$) after correction for dilution (Fig. 3) and concluded that there was no appreciable excess of gallium in the structure. Virtually all the gallium occurred in the $^{IV}Ga(O)_4$ site of the molecule.

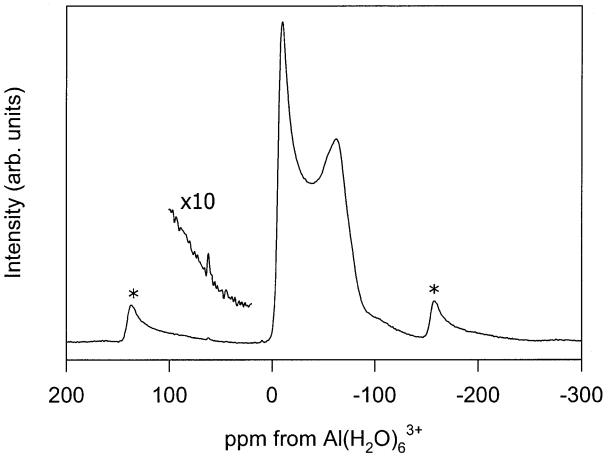

Fig. 2. ^{27}Al-MAS-NMR spectra of the $Na[GaO_4Al_{12}(OH)_{24}(H_2O)_{12}(SeO_4)_4](H_2O)_x$ crystals used to prepare experimental solutions. The inset shows the very small peak at 62 ppm that corresponds to tetrahedrally coordinated aluminum in impurity Al_{13} in the solid, which are present at concentrations of less than 0.5%. Asterisks denote spinning sidebands.

We began an ^{17}O-NMR experiment using the method described in Phillips et al. (2000) and Casey et al. (2000). Briefly, crystals were ground with $BaCl_2$ and then extracted with 2 mL of isotopically normal water, followed by agitation and filtration. This extraction causes the crystals to dissolve and release $GaAl_{12}$ molecules to solution but retains the selenate as a barium–selenate precipitate. This solution, and a solution containing 0.5 mol/L $MnCl_2 + H_2^{17}O$ (35%, Isotec Laboratories) were separately brought into thermal equilibrium in a water bath at the desired temperature before we mixed together 1.0 mL of the filtrate with 1.0 mL of the $H_2^{17}O$-enriched solution. This procedure resulted in $\approx$0.010 mol/L solution of isotopically normal $GaAl_{12}$ in a 0.25 mol/L solution of $MnCl_2$ at pH $\approx$ 4.8 $\pm$ 0.1 (Table 1) that was enriched to $\approx$17% in $H_2^{17}O$. After measuring pH, we transferred the mixture to a thermally equilibrated NMR tube and then into the spectrometer. The time from mixing of the solutions to collection of the first spectrum was usually $\sim$10 min.

The pH of the solution was heavily buffered, and all experiments gave similar initial pH values (Table 1). With time, the pH drifted to lower values as the molecule decomposed slightly. The drift during a single day, which covered measurement of exchange rates of the more labile hydroxyl site, was generally less than 0.2 units, and commonly $\sim$0.1 units, of pH (Table 1). Drift continued over several days to weeks during exchange of the less reactive hydroxyl site, and some samples exhibited a total drift of 0.7 pH units. Therefore, the pH control for exchange of the first hydroxyl site was much better than for the second, less reactive site. The solution pH was determined with a combination electrode that was calibrated on the concentration scale by titrating solutions of 0.25 mol/L $MnCl_2$ + 0.25 mol/L $BaCl_2$ with a strong acid. The apparent ionic strength (I_a) of each experimental solution was $\sim$1.7 mol/L.

2.2. Temperature Control

Temperatures were monitored by placing a copper-constantan thermocouple into the coaxial insert of a sample tube and inserting this apparatus into the spectrometer. The precision and accuracy of the spectrometer temperature setting is equal to or better than $\pm$0.5 K. For experiments to determine the rates of exchange of the less labile hydroxyl site in the $GaAl_{12}$ complex, we placed the samples in a constant-temperature bath with a temperature uncertainty of $\pm$0.2 K. For calculating rate coefficients, we used a value of $\pm$0.5 K as a standard deviation (1σ) for temperature variations in a single experiment, which is very conservative.

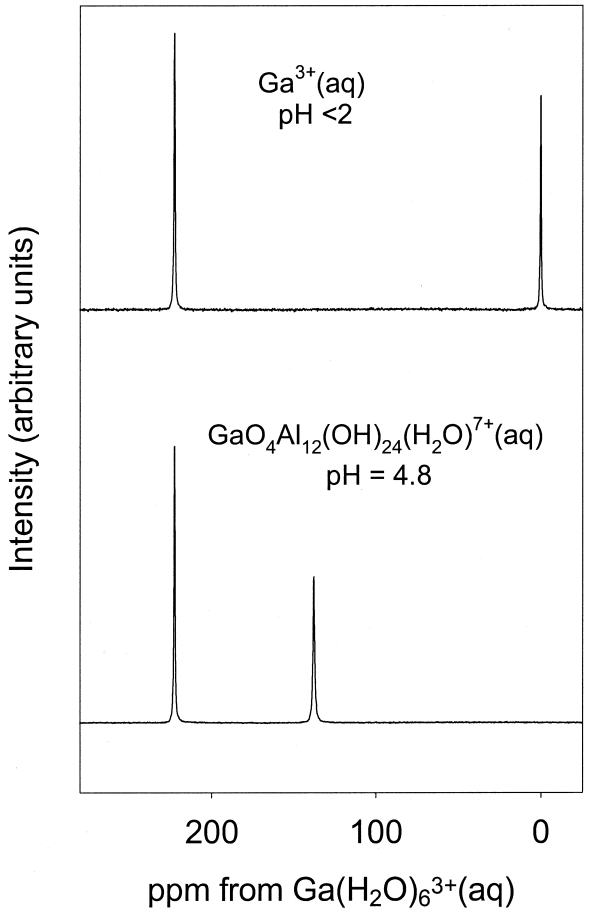

Fig. 3. ^{71}Ga-NMR spectra of an aqueous solution after extraction of $GaAl_{12}$ molecules by dissolution of $Na[GaO_4Al_{12}(OH)_{24}(H_2O)_{12}(SeO_4)_4](H_2O)_x$ crystals (bottom) and after subsequent acid digestion of the dissolved $GaAl_{12}$ complexes (top). In both, the peak in the spectrum at 223 ppm corresponds to $Ga(OH)_4^-$(aq) in an external coaxial standard. The ratios of the integrated intensity of the ^{71}Ga-NMR peak at 138 ppm (bottom) or at 0 ppm (top), divided by the intensity of the $Ga(OH)_4^-$(aq) standard, are similar in both cases. The peak at 138 ppm (bottom) corresponds to the GaO_4 group in the dissolved $GaAl_{12}$ complex and that at 0 ppm (top) corresponds to Ga^{3+}(aq). The similar ratio of intensities observed before and after digestion indicates that the $Ga(O)_4$ site of the $GaAl_{12}$ complex contains virtually all the dissolved gallium in the extracted solutions.

2.3. NMR Spectroscopy

The solution-state ^{17}O-, ^{27}Al-, and ^{71}Ga-NMR experiments were conducted at conditions similar to our previous experiments on the Al_{13} complex (Phillips et al., 2000). Briefly, NMR measurements were made with a Bruker Avance spectrometer that is based on an 11.7 T magnet (ν_o = 67.8 MHz for ^{17}O; ν_o = 130.3 MHz for ^{27}Al; ν_o = 152.5 MHz for ^{71}Ga) fitted with a 10-mm broadband probe. The ^{17}O-NMR spectra were taken with single-pulse excitation with 20-μs pulses ($\pi/2 \approx 40$ μs) and recycle delays of 6 ms. Depending on the sample, 20,000 to 80,000 acquisitions were required to establish an adequate signal-to-noise ratio. The ^{71}Ga and ^{27}Al spectra were taken with longer relaxation delays (0.15 and 1 s, respectively), but under broadly similar conditions.

2.4. ^{17}O-NMR Measurements

A coaxial insert of 0.3 mol/L $TbCl_3$ in isotopically normal water was included in all ^{17}O-NMR experiments. This insert gives a peak near -100 ppm in the ^{17}O-NMR spectra that corresponds to bulk waters and waters bound to the Tb^{3+} ion that are in rapid-exchange equilibrium (see Cossy et al., 1988). This peak corresponds to a constant number of ^{17}O nuclei throughout the experiment so that changes in the absolute concentrations of ^{17}O in the various peaks could be assessed during an experiment with dissolved $GaAl_{12}$. We also obtained line-shape parameters from least-squares fits of the frequency-domain data to a sum of Lorentzian curves. Usually, three curves could adequately fit the data (including the peak corresponding to the $TbCl_3$ insert), except at long times where two curves are needed to fit the bound-hydroxyl peak, as we discuss below.

The rates of exchange of the μ_2-OH sites were measured from the rate of change in intensity of the peaks in the ^{17}O-NMR spectra. These changes in intensity are fit to a form of the McKay equation (see Casey et al., 2000) to derive rate coefficients. Rates of exchange of η^1-OH_2 sites between the $GaAl_{12}$ complex and solvent were measured with the dynamic ^{17}O-NMR line-broadening technique (Swift and Connick, 1962; Hugi-Cleary et al., 1985, 1987) on isotopically equilibrated samples. In this method, ^{17}O-NMR transverse relaxation times T_2 were obtained directly from the NMR line width: $T_2 = 1/(\pi \cdot FWHM)$, where *FWHM* is the full width at half maximum of the ^{17}O-NMR resonance. The ^{17}O-NMR resonance from bulk water was broadened beyond detection by interaction with Mn(II) species present in the solution.

In estimating rate coefficients, we assigned uncertainties in the peak intensities of 0.02 absolute (1σ, total intensity normalized to unity) and 10% in the raw peak widths. These values comfortably span the range of values that are consistent with reasonable adjustments in spectrum phasing and baseline correction. In samples containing Mn(II), ^{17}O and ^{71}Ga peaks for all complexed species exhibited a downfield shift of about +12 to +22 ppm from their expected positions relative to external frequency standards. The ^{17}O-NMR peak positions for solutions that contained Mn(II) were referenced internally to the bound waters (η^1-OH_2), which were taken to be +22 ppm, similar to the Al_{13} complex (Thompson et al., 1987). The ^{71}Ga-NMR peak positions are reported relative to $Ga(H_2O)_6^{3+}$(aq) at 0 ppm.

2.5. ^{27}Al and ^{71}Ga-NMR Measurements

To demonstrate that the $GaAl_{12}$ molecule is kinetically stable over a typical experiment and that our extraction procedure provides a monospecific solution, we monitored the intensity of the peak corresponding to the $^{IV}Ga(O)_4$ site in the $GaAl_{12}$ molecule relative to the peak corresponding to $Ga(OH_4)^-$(aq) in a coaxial standard in experiments at 313 K. We observed no measurable changes in the relative intensities or peak positions over ~3 weeks, which spans the duration of a typical experiment at this temperature. We also saw no evidence for formation of high-molecular-weight polyoxocations, such as the gallium equivalent of the "Al_{P2}" polymer found by Fu et al. (1991) at higher temperatures and assigned the stoichiometry $Al_{30}O_8(OH)_{56}(H_2O)_{26}^{18+}$(aq) by Rowsell and Nazar (2000). To produce this Al_{P2} polymer, the authors created Al_{13} from forced titration of $AlCl_3$ solutions at high temperature. In our method, we dissolve crystals containing the molecule at low temperatures, which generates a kinetically stable, monospecific solution of $GaAl_{12}$.

The solid-state ^{27}Al-NMR spectra (Fig. 2) were collected on a Chemagnetics CMX-400 NMR spectrometer at 104.3 MHz. The ^{27}Al-NMR spectra were taken with single-pulse excitation with 0.5-μs pulses (nonselective π = 12 μs), relaxation delay of 0.2 s, and 4000 acquisitions. There was no change in relative intensity upon increasing the relaxation delay to 2 s. The samples were spun at 15.4 kHz with 4 mm outer diameter ZrO_2 rotors, and all resonances are reported relative to $\delta^{27}Al = 0$ ppm for $Al(H_2O)_6^{3+}$(aq) in an external dilute solution of $Al(NO_3)_3$.

3. RESULTS

3.1. ^{17}O-NMR Peak Assignments

The present results are broadly similar to those of our previous study of Al_{13} (Phillips et al., 2000). The ^{17}O-NMR spectrum exhibits a relatively narrow peak near +20 ppm (Fig. 4) in our first spectrum of a solution. This peak exhibits a

Table 1. Experimental results for exchange of the two μ_2-OH sites in $GaAl_{12}$. The pH values were measured shortly after mixing the $GaAl_{12}$ and $H_2{}^{17}O$ solutions (initial) and after the experiment (final) at the indicated total elapsed time since mixing. The characteristic times for exchange of the hydroxyl oxygens are derived from least-squares fits of the data to Eqn. 4. Sample 30-80 was used to determine rates of water exchange only. The uncertainties are based on Monte Carlo error analysis with 1σ (Intensity) = 0.02.

Sample	Temperature (K)	pH initial	pH final	Time (h)	τ_1 ($\pm 1\sigma$) (1000 s)	τ_2 ($\pm 1\sigma$) (1000 s)
30-80		4.90				
30-94	301	4.73	4.32	1128	43.5 (±0.5)	1394 (±40)
32-13	305	4.83	4.17	960	16.9 (±0.2)	623 (±20)
32-15	309	4.84	4.26	840	12.6 (±0.1)	428 (±12)
32-17	309	4.71	4.10	696	12.3 (±0.1)	450 (±12)
32-18	313	4.71	4.12	385	7.8 (±0.1)	192 (±5)
32-27	313	4.46	4.23	7	9.0 (±0.1)	ND
32-33	313	4.92	4.19	624	5.4 (±0.1)	102 (±3)
32-37	313	4.15	3.98	432	8.4 (±0.1)	214 (±7)
32-40	313	4.29	3.975	385	8.5 (±0.1)	221 (±5)
32-20	317	4.54	4.04	217	5.6 (±0.1)	100 (±3)

ND, not done.

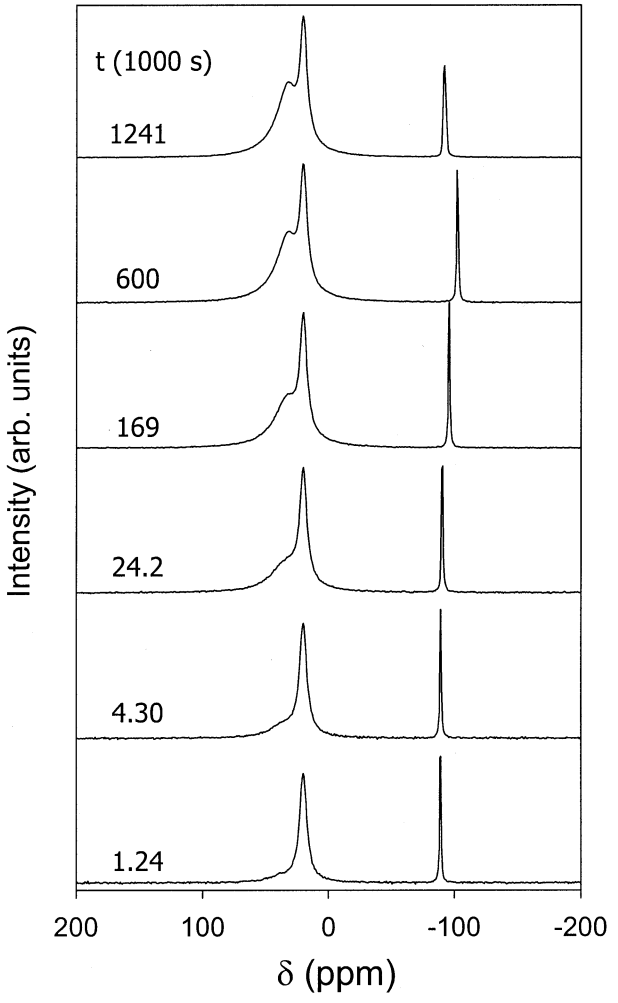

Fig. 4. ^{17}O-NMR spectra at 313 K as a function of time for a ≈0.010 mol/L solution of $GaAl_{13}$ with 0.25 mol/L Mn(II) added to remove the bulk water peak. Vertical scaling is normalized to the integrated intensity of the peak near −100 ppm, which corresponds to an external, coaxial $TbCl_3$(aq) insert that was used as an intensity standard. The peak near +22 ppm corresponds to water molecules (η^1-OH_2 sites) bound to the $GaAl_{12}$ complex. The broader, downfield peak that increases in intensity with time arises from the two μ_2-OH sites in the molecule, which react at different rates.

constant intensity relative to that of the peak near −100 ppm that arises from the aqueous $TbCl_3$ coaxial insert. Throughout the course of an experiment, the intensity ratio of these peaks at +22 and −100 ppm varies less than a few percent (Fig. 5, bottom). These results are consistent with our assignment of the narrower peak at +20 ppm to the 12 equivalent η^1-OH_2 groups in the $GaAl_{12}$ complex (see Phillips et al., 2000). These terminal water molecules isotopically equilibrate with the ^{17}O-enriched bulk solutions in fractions of a second (vide infra), so the peak at +22 ppm appears virtually instantaneously in our experiments and maintains a constant absolute intensity.

After a period of reaction that varies with temperature, a broader shoulder develops that is centered near +35 ppm (Fig. 4). This peak increases in intensity until it eventually attains an intensity equal to the peak at +22 ppm; at this point, the ratio of intensities are equal ($[R(t) \approx 1; R(t) = (I_{\delta=35}/I_{\delta=22})]$, where $I_{\delta=22}$ is the integral of the curve fit to the peak near δ = 22 ppm). The amount of time needed to reach the condition $R(t)$ = 1 varies considerably with temperature, as does the width of the peak at +35 ppm. After attaining $R(t)$ = 1, the rate of intensity increase at +35 ppm then slows considerably (Fig. 5, top), and the width of this peak appears to decrease significantly until an intensity ratio of $R(t) \approx 2$ is reached.

Fits of the ^{17}O-NMR spectra of $GaAl_{12}$ at long equilibration times [$1.5 < R(t) \leq 2$] were improved by addition of a fourth curve also near +35 ppm but having a width ~56% of that initially fit to the broad peak at conditions early in an experiment [$0 < R(t) \leq 1$]. When fit to a single curve, the width of the peak near +35 ppm appears to remain approximately constant from the start of the experiment [$R(t) = 0$] to near $R(t) = 1$, then decreases significantly until isotopic equilibration is reached [$R(t) = 2$], which is consistent with increasing intensity with time of a more narrow component at +35 ppm between $R(t) = 1$ and 2.

All the spectral changes that occur between $R(t) = 1$ and $R(t) = 2$ can be attributed solely to an exponential increase in the intensity of the second, narrower component at +35 ppm that eventually reaches a value approximately equal to that of the peak at +22 ppm. After reaching $R(t) = 2$, the absolute intensities of the peak at +22 ppm and the broader component

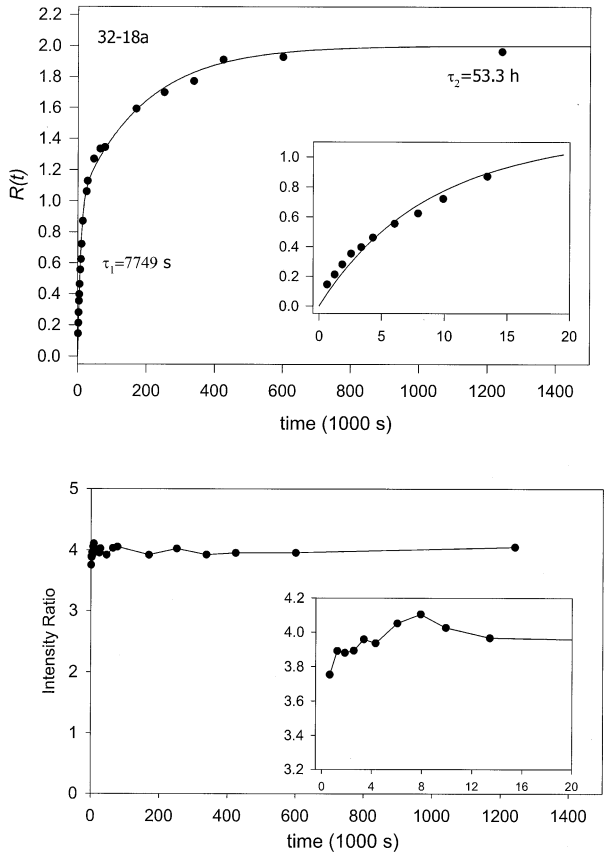

Fig. 5. (Top) The intensity ratio, $R(t)$, of the peaks at +35 ppm (assigned to μ_2-OH sites) and at +22 ppm (assigned to η^1-OH_2 sites) as a function of time after addition of water enriched to ≈17% in ^{17}O at 313 K. The biexponential behavior indicates differing rates of exchange for the two types of bound hydroxyl, μ_2-OH and μ_2-OH′ identified in Figure 1. The lines correspond to least-squares fits of Eqn. 4 to the data, and the inset diagram shows the early part of the curve at an expanded scale. (Bottom) For the same experiment, the ratio of intensities of peaks assigned to the η^1-OH_2 sites in the $GaAl_{12}$ complex (+22 ppm) divided by the intensity of the $TbCl_3$(aq) coaxial standard (−100 ppm) as a function of time. The inset diagram shows the ratio for the early part of the experiment at an expanded scale.

at +35 ppm remain constant (Fig. 5). Likewise, all peak widths remain constant.

Our interpretation that the apparent narrowing of the peak at +35 ppm with time is due to increasing intensity of a narrower component is substantiated by the temperature dependence of the fitted peak widths for isotopically equilibrated samples. In Figure 6, we show an Arrhenius plot with the transverse relaxation rates determined from the fitted peak widths [$T_2 = 1/(\pi \cdot FWHM)$] for the two components. Under these conditions, the peak width is dominated by quadrupolar relaxation. The fact that the slopes for these two peaks have different intercepts indicates that the two corresponding sites have distinct quadrupolar coupling constants. The identical slopes reflect the temperature dependence of the molecular rotational correlation time, τ_c (see below), which should be the same for two sites in the same molecule, as we observe (Fig. 6).

The ability to distinguish two components in the peak at +35 ppm contrasts these results with those of our earlier study of

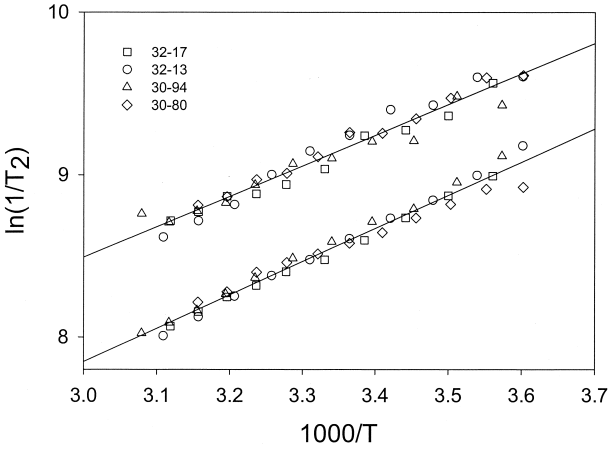

Fig. 6. Arrhenius plot of the transverse relaxation rates ($1/T_2$) for the two hydroxyl resonances of $GaAl_{12}$. The T_2 values were obtained from the widths of two Lorentzian curves fit to the peak near +35 ppm [$T_2 = 1/(\pi \cdot FWHM)$] for isotopically equilibrated samples with the constraint that the intensity of the broader curve equal that of the peak at +22 ppm, due to the bound waters. This interpretation accounts for the observation that the peak at +35 ppm appears to narrow as $R(t)$ increases from 1 to 2 (Fig. 4). Lines are linear least-squares fits to the data and represent the temperature dependence of quadrupolar relaxation for the two distinct hydroxyl sites.

Al_{13} (Phillips et al., 2000), which was undertaken at lower temperatures because of the much faster rates of oxygen exchange for Al_{13}. At lower temperatures, the peak at +35 ppm is much broader and more difficult to measure accurately. Recent instrumental improvements have also enhanced our ability to measure large peak widths. We assign the two kinetically distinct resonances at +35 ppm to the two structurally distinct μ_2-OH sites within the $GaAl_{12}$ molecule, consistent with our previous work (Phillips et al., 2000).

3.2. Rates of Exchange of η^1-OH_2 Sites

The chemical exchange rates of the η^1-OH_2 sites were obtained by fitting the ^{17}O-T_2 values for the peak at 22 ppm (Fig. 7) to Eqn. 1, which incorporates the contributions from chemical exchange and quadrupolar relaxation

$$\frac{1}{T_2} = \frac{1}{\tau} + \frac{1}{T_{2,q}}, \tag{1}$$

where τ is the mean lifetime of a water molecule in the inner coordination sphere and $1/T_{2,q}$ is the intrinsic quadrupolar relaxation rate. An Arrhenius-like relation is used to approximate the rates of quadrupolar relaxation,

$$\frac{1}{T_{2,q}} = W_{q,298} e^{\frac{E_q}{R}\left[\frac{1}{T}-\frac{1}{298}\right]}, \tag{2}$$

where E_q and $W_{q,298}$ are fitting parameters (see Casey et al., 2000; Phillips et al., 2000).

The temperature dependence of k_{ex} (s^{-1}), the first-order rate coefficient for exchange of water molecules from the inner coordination sphere to the bulk solution, takes the form of the Eyring equation,

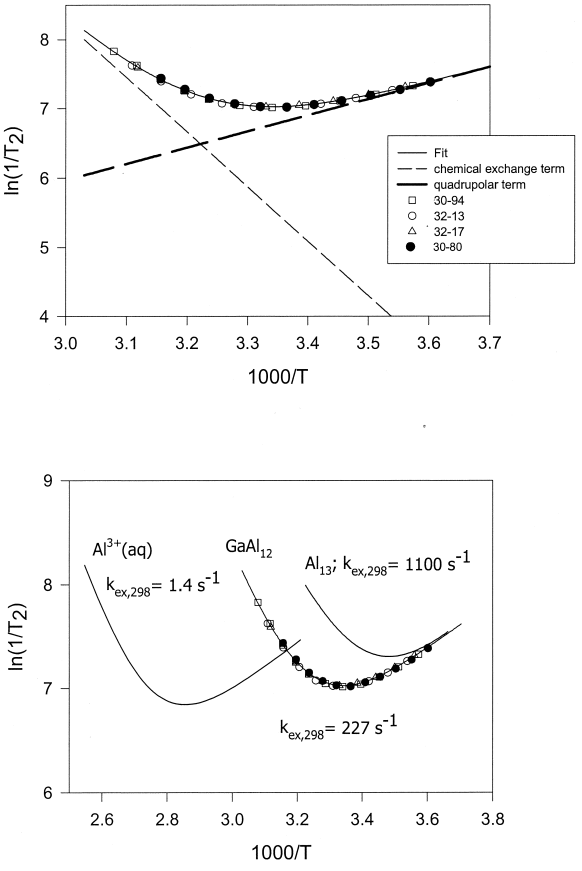

Fig. 7. (Top) Arrhenius plot of the ^{17}O NMR transverse relaxation rate ($1/T_2$) values for bound waters in the $GaAl_{12}$ complex. Different symbols correspond to distinct samples for chemical conditions reported in Table 1. Values of $1/T_2$ are obtained from the width of the peak at +22 ppm returned from unconstrained least-squares fits of the spectra to a sum of Lorentzian curves. The solid line is a least-squares fit of the data to Eqns. 1 to 3, comprising contributions from chemical exchange (coarse-dashed line) and quadrupolar relaxation (dotted line). (Bottom) Temperature variations of the $1/T_2$ values for the $GaAl_{12}$ complex compared with values determined for the $Al(H_2O)_6^{3+}$(aq) complex (Hugi-Cleary et al., 1985) and the Al_{13} complex (Casey et al., 2000; Phillips et al., 2000).

$$k_{ex} = \frac{1}{\tau} = \frac{k_b \cdot T}{h} e^{\frac{\Delta S^{\ddagger}}{R}} e^{\frac{-\Delta H^{\ddagger}}{RT}}, \tag{3}$$

where k_b is Boltzmann's constant and the exponential terms include the activation entropy [$\Delta S^{\ddagger}$] and activation enthalpy [$\Delta H^{\ddagger}$] for chemical exchange. The parameters T, R, and h are absolute temperature, the gas constant, and Planck's constant, respectively. The results of least-squares fits to the data are presented in Table 2 and are presented graphically in Figure 7.

3.3. Rates of Exchange of μ_2-OH Sites

To account for the nonlinear variation of the intensity of the peak near 35 ppm with time, the ratio of the intensities relative to the peak at +22 ppm (assigned to the η^1-OH_2 sites) were fit to a rate law that is the sum of two exponential terms. Physically, each of these terms represents exchange of one of the two sets of structurally distinct μ_2-OH sites:

Table 2. Rate parameters for exchange of η^1-OH_2 sites on the $GaAl_{12}$ molecule with water molecules in the bulk solution, derived from a least-squares fit of the temperature variation of the peak widths at +22 ppm to Eqns. 1 to 3 (Fig. 7). Rate parameters and uncertainties ($\pm 1\sigma$) for the aggregated data are assigned from Monte Carlo simulation assuming a 0.5°C uncertainty in temperature and 10% in the raw line width, which are conservative.

Sample	k_{ex}^{298} (s^{-1})	$\Delta H^{\ddagger}$ (kJ mol^{-1})	$\Delta S^{\ddagger}$ (JK^{-1} mol^{-1})	$W_{q,298}$ (s^{-1})	$E_{a,q}$ (kJ mol^{-1})
30-80	224.4	67	24		
30-94	228.5	64	65		
32-13	206.3	65	19		
32-17	188.2	69	29		
All data	227 (±40)	63 (±7)	13 (±21)	891 (±61)	20 (±3)

$$R(t) = \frac{I_{OH}(t)}{I_{\eta-OH_2}} = 2 - e^{-\frac{t}{\tau_1}} - e^{-\frac{t}{\tau_2}}. \tag{4}$$

In Eqn. 4, t is the time elapsed since addition of $H_2{}^{17}O$ to the solution, and τ_1 and τ_2 are the characteristic times for exchange of the hydroxyl sites, with $\tau_1 \ll \tau_2$. The constant 2 in Eqn. 4 derives from the stoichiometry of the complex; that is, there are two sets of 12 μ_2-OH sites in a single molecule and one set of 12 η^1-OH_2 sites. A least-squares fit of $R(t)$ values to Eqn. 4 yields values of the characteristic times τ_1 and τ_2 as a function of temperature and solution pH (Table 1; Fig. 5, top). The characteristic times, τ_1 and τ_2, can be reduced to first-order rate coefficients for chemical exchange by applying the McKay equation (see Casey et al., 2000) so that

$$k_1 = \frac{1}{\tau_1}, \qquad k_2 = \frac{1}{\tau_2}. \tag{5}$$

These pseudo–first-order rate coefficients are numerically equivalent to first-order rate coefficients for oxygen exchange between the aqueous solution and the μ_2-OH sites.

Over the experimental temperature range, the values of k_1 and k_2 vary considerably in accordance with the Arrhenius rate law (Fig. 8):

$$k_i(t) = A_i \cdot e^{\frac{-E_{a,i}}{R \cdot T}}, \tag{6}$$

from which activation energies (E_a) are derived for each ($i = 1$, 2) site and converted into activation enthalpies and entropies via the Eyring equation (Eqn. 3). Extrapolation of the rate coefficients in Table 1 to 298 K yields $k_{ex,1}^{298} = 1.8(\pm 0.11) \cdot 10^{-5}\ s^{-1}$ and $k_{ex,2}^{298} = 4.1(\pm 0.2) \cdot 10^{-7}\ s^{-1}$. The corresponding activation parameters are as follows: $\Delta H_1^{\ddagger} = 98(\pm 3)$ kJ mol^{-1} and $\Delta S_1^{\ddagger} = -8.1(\pm 9)$ J mol^{-1} K^{-1}, $\Delta H_2^{\ddagger} = 125(\pm 4)$ kJ mol^{-1}, and $\Delta S_2^{\ddagger} = 54(\pm 12)$ J mol^{-1} K^{-1}.

3.4. Variation in Rates with pH

We observed no significant pH dependence to exchange rates, although the data extend over only a small range. Over the range of ~0.75 pH units in experiments at 313 K (Table 1), we observed less than ≈30% variation in the rates. Over this range in pH values, a first-order dependence of rate on dissolved proton concentration would cause rates to vary by a factor greater than five.

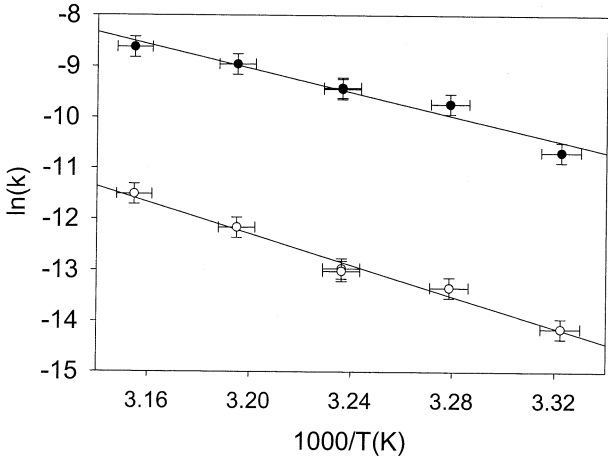

Fig. 8. An Arrhenius plot of $\ln(k_{ex,i})$ against $1/T$ (K) for exchange of the two μ_2-OH sites in the $GaAl_{12}$ molecule. Uncertainties of ± 0.5 K were assigned to temperature and ± 0.2 to $\ln(k_{ex,i})$ in the plot. Both of these uncertainties are conservative. The lines correspond to full least-squares fits of the data to Eqn. 3.

The experimentally accessible pH range in the acid direction is limited by decomposition of the $GaAl_{12}$ molecule so that it was impossible to maintain pH < 4.0 long enough to conduct an experiment. After adjusting the pH in the basic direction, we found that the extent of exchange of the two μ_2-OH sites deviated considerably from double-exponential growth. We interpret the result to indicate partial polymerization of the $GaAl_{12}$ molecule during transient periods of high pH as the titrant mixed (for comparison with Al_{13}, see Furrer et al., 1992b). For this reason, we did not use rate data from solutions where the pH was raised (sample 32-33) to estimate activation parameters. We find no evidence for steady exchange of the ^{17}O into the μ_4-O sites in the $GaAl_{12}$, as we also observed for the Al_{13} molecule (Phillips et al., 2000). Although the μ_4-O in $GaAl_{12}$ should exhibit a larger ^{17}O peak width than for Al_{13}, on the basis of its larger quadrupolar coupling in the solid state, 3.25 MHz; (our unpublished data) vs. 1.2 MHz for Al_{13} (Thompson et al., 1987), it should be easily resolved if significant exchange occurred.

3.5. Assignment of the Hydroxyl Resonances

The observed parallel temperature variation of the line widths fit to the two hydroxyl components (Fig. 6) is consistent with two sites having different C_q values but the same τ_c variation with temperature. For ^{17}O in the regime of extreme narrowing but slow chemical exchange, the NMR peak widths are dominated by quadrupolar relaxation:

$$\frac{1}{T_2} = \pi \cdot FWHM = \frac{3}{40}\frac{2I+3}{I^2(2I-1)}\left[1+\frac{\eta^2}{3}\right]\cdot[2\pi C_q]^2\cdot\tau_c, \quad (7)$$

where I is the spin quantum number ($I = 5/2$ for ^{17}O), C_q is the nuclear quadrupolar coupling constant (the product of the nuclear quadrupolar moment and the maximum component of the electric-field gradient at the nucleus, measured in Hertz) and η the asymmetry of the electric-field gradient (unitless), and τ_c is the molecular rotational correlation time (measured in seconds) (Abragam, 1961). The temperature dependence of the line width arises from changes in τ_c.

On this basis, we can assign the more labile hydroxyl to that site on $GaAl_{12}$ with the larger electric-field gradient. The ratio of line widths ($\sim$1.8) suggests that the more labile site exhibits a C_q value $\sim$35% larger than that of the less reactive site. Thompson et al. (1987) estimated $\tau_c = 130$ ps for the Al_{13} molecule at 296 K from measurements of the octahedral ^{27}Al NMR peak width and of the C_q value of the same site in the crystal by solid-state NMR. Use of this τ_c value for $GaAl_{12}$, which is identical in size to Al_{13}, yields C_q values of 8.7 MHz for the more labile hydroxyl and 6.5 MHz for the more slowly exchanging site. However, we are unable to distinguish the two μ_2-OH sites in solid-state ^{17}O-NMR spectra of selectively enriched crystals, suggesting that dynamic and/or structural differences between the crystalline and dissolved forms might affect the C_q values.

Reexamination of our earlier ^{17}O-NMR data for Al_{13} (Casey et al., 2000; Phillips et al., 2000) also shows an apparent decrease in the width of the peak near $+35$ ppm between $R(t) = 1$ and $R(t) = 2$, although these widths are larger and more difficult to measure accurately because of the lower temperatures employed. This result suggests a similar assignment for Al_{13}, as discussed above for $GaAl_{12}$.

4. DISCUSSION

4.1. Comparison of Oxygen-Exchange Rates in the Al_{13} and $GaAl_{12}$ Molecules

There are clear differences in oxygen labilities between the Al_{13} and $GaAl_{12}$ molecules, even at sites that are well removed from the site of $^{IV}Ga(III)$ substitution for $^{IV}Al(III)$. For example, the pseudo–first-order rate coefficient for exchange of η^1-OH_2 sites on the $GaAl_{12}$ molecule [$k_{ex}^{298} = 227(\pm 40)\ s^{-1}$] is $\approx$5 times smaller than that for the Al_{13} molecule [$k_{ex}^{298} = 1100(\pm 300)\ s^{-1}$] (Phillips et al., 2000). One can see in Figure 7 (bottom) that the differences in the raw data are much larger than the experimental uncertainties. On the other hand, the activation enthalpies for η^1-OH_2 site exchange [Al_{13}: $53(\pm 12)$ kJ $\cdot$ mol^{-1} and $GaAl_{12}$: $63(\pm 7)$ kJ $\cdot$ mol^{-1}] are probably identical to within the experimental uncertainties.

More striking are the differences in the rates of exchange of the two μ_2-OH sites between the Al_{13} and $GaAl_{12}$ molecules. First, the two μ_2-OH sites are *generally* less labile in the $GaAl_{12}$ complex than in Al_{13}. Characteristic times for exchange of the two μ_2-OH sites in the $GaAl_{12}$ molecule at 298 K are $\approx$15.5 and $\approx$680 h, respectively, whereas the corresponding times are $\approx$1 min and $\approx$17 h for the Al_{13} molecule (see Casey et al., 2000; Phillips et al., 2000). As discussed above, the line width data indicate that rates for both μ_2-OH sites change, rather than a large difference for one site and little change in the other. Second, the decrease in reactivity of the two μ_2-OH sites is not uniform as Ga(III) substitutes for Al(III) in the central tetrahedral site. The $k_{ex,1}^{298}$ value for the Al_{13} molecule is larger than $k_{ex,1}^{298}$ for the $GaAl_{12}$ complex by a factor of $\approx$900. Similarly, for the less labile hydroxyl site, the $k_{ex,2}^{298}$ value for the Al_{13} molecule is $\approx$40 times larger than for the $GaAl_{12}$ complex. The difference of labilities of the two μ_2-OH sites within each molecule is reduced considerably when Ga(III) is substi-

tuted for Al(III) in the structure. For the Al_{13} complex, ($k_{ex,1}^{298}/k_{ex,2}^{298}$) $\approx 10^3$, but for the $GaAl_{12}$ molecule, ($k_{ex,1}^{298}/k_{ex,2}^{298}$) ≈ 44.

This unequal change in labilities upon ^{IV}Ga(III) substitution for ^{IV}Al(III) is also manifested in the activation parameters. One troubling result from our study of the Al_{13} complex was that the $\Delta H^{\ddagger}$ values for the two distinct μ_2-OH sites differ considerably and that the $\Delta H_1^{\ddagger}$ and $\Delta S_1^{\ddagger}$ are much higher than values reported for uncatalyzed dissociation of hydroxyl bridges in other polyoxocations. Activation enthalpies for dissociation of μ_2-OH sites in inert transition-metal dimers tend to fall in the range $\Delta H^{\ddagger} = 100(\pm 20)$ kJ mol^{-1} with activation entropies around zero (e.g., Springborg, 1988; Richens, 1997). The activation parameters for exchange of the more labile μ_2-OH site in the Al_{13} were as follows: $\Delta H_1^{\ddagger} = 204(\pm 12)$ kJ mol^{-1} and $\Delta S_1^{\ddagger} = 403(\pm 43)$ J mol^{-1} K^{-1}, compared with $\Delta H_2^{\ddagger} = 104(\pm 20)$ kJ mol^{-1} and $\Delta S_2^{\ddagger} = 5(\pm 4)$ J mol^{-1} K^{-1} for the less reactive μ_2-OH site (Casey et al., 2000; Phillips et al., 2000).

In contrast, the activation parameters for μ_2-OH site exchange in the $GaAl_{12}$ complex are similar to one another. The more rapidly reacting μ_2-OH site in the $GaAl_{12}$ molecule has $\Delta H_1^{\ddagger} = 125(\pm 12)$ kJ mol^{-1}, which is considerably smaller than $\Delta H_1^{\ddagger}$ in the Al_{13} molecule but similar to $\Delta H_2^{\ddagger}$ for both $GaAl_{12}$ and Al_{13} [98 and 125(± 4) kJ mol^{-1}, respectively]. Both $\Delta H_1^{\ddagger}$ and $\Delta H_2^{\ddagger}$ for $GaAl_{12}$ are near the range observed for inert-metal dimers.

4.2. Structural Differences Between the $GaAl_{12}$ and Al_{13} Molecules

The remarkable differences in oxygen-exchange rates between the $GaAl_{12}$ and Al_{13} are not reflected in any large differences in the structures of these molecules in crystals. Parker et al. (1997) presents a detailed comparison of the structures of the $GaAl_{12}$ and Al_{13} sulfate salts, and the important crystallographic features are summarized in Table 3. By using the numbering scheme of Johansson (1962a,b) and Parker et al. (1997), oxygens in the μ_2-OH′ group are denoted O(1), oxygens in the μ_2-OH are O(4), oxygens in the μ_4-O are O(2), and oxygens in the η^1-OH_2 are O(3). The bond angles in the $GaAl_{12}$ and Al_{13} are identical to within experimental uncertainties (Table 3).

Not surprisingly, substitution of ^{IV}Ga(III) for ^{IV}Al(III) causes a conspicuous increase in the bond length between the tetrahedral cation and the μ_4-O oxy site from 1.831(4) Å in Al_{13} to 1.879(5) Å in $GaAl_{12}$ (Table 3). Lengthening of this bond [$^{IV}M_T$-O(2)] causes an associated contraction of the adjacent Al_o-O(2) bond from 2.026(4) to 2.009(6) Å, which is significant. Because we see no evidence that the μ_4-O exchanges with bulk solution in our experiments, the effect of these structural changes on reaction rates cannot yet be assessed. Logically, the structural effects of gallium substitution will be reflected in the dissolution rate of the $GaAl_{12}$ molecule, which has not been measured and is probably reflected in the Brønsted acidity of this μ_4-O site, which is crucial for dissolution (see Casey et al., 2000).

The two sets of hydroxyl bridges (μ_2-OH and μ_2-OH′; Fig. 1) differ in exchange rates by factors of $\approx$44 in the $GaAl_{12}$ and $\approx$1000 for the Al_{13}, yet the two sets of oxygens in these hydroxyl bridges have identical inner coordination sphere neighbors of one proton and two aluminums. In the Al_{13} molecule, Al-O bond lengths in both the μ_2-OH and μ_2-OH′ bridges are 1.857(6) Å (Table 3). Upon substitution of ^{IV}Ga(III) for ^{IV}Al(III), the Al–O bonds in the μ_2-OH bridges apparently lengthen slightly to 1.869(7) Å, but this small difference is probably insignificant. The μ_2-OH′ bridges [Al_o-O(1)] are virtually unaffected by substitution, as the Al–O bond lengths are 1.857(6) Å in the Al_{13} complex and 1.852(6) Å in the $GaAl_{12}$ molecule; these are identical to within experimental uncertainties (Table 3). Apparently the difference in reactivity of these various oxygen sites in the two molecules are associated with changes in structure that are too subtle to detect via X-ray crystallography.

Table 3. Structural data for Al_{13} and $GaAl_{12}$ sulfate salts having the nominal composition $Na[M_TO_4(Al_O)_{12}(OH)_{24}(H_2O)_{12}(SO_4)_4](H_2O)_{10}$, where M = Al(III) or Ga(III). The data are from Parker et al. (1997), and the atom numbering scheme is described there, in Johansson (1962), and in Figure 1. The subscript abbreviations are T = tetrahedral and O = octahedral. The standard deviation for each bond parameter value is given in parentheses and corresponds to the last place in the value. The *oxy* site that is nearest the relevant bond is identified in the right-hand column. See Figure 1.

Moiety	M = Al(III) Bond length (Å)	M = Ga(III) Bond length (Å)	Structural site
M_T-O(2)×4	1.831(4)	1.879(5)	μ_4-O
Al_O-O(1)×2	1.857(6)	1.852(6)	μ_2-OH′
Al_O-O(2)	2.026(4)	2.009(6)	μ_4-O
Al_O-O(3)	1.961(4)	1.962(6)	η^1-OH_2
Al_O-O(4)×2	1.857(6)	1.869(7)	μ_2-OH
	Bond angles (degrees)		
O(2)-M_T-O(2′)×6	109.5(2)	109.5(2)	
O(1)-Al_O-O(1′)	78.0(2)	77.5(2)	
O(1)-Al_O-O(2)×2	95.4(2)	95.4(2)	
O(1)-Al_O-O(3)×2	92.3(2)	92.7(2)	
O(1)-Al_O-O(4)×2	94.2(2)	94.5(2)	
O(1)-Al_O-O(4′)×2	171.6(2)	171.1(3)	
O(2)-Al_O-O(3)	170.1(2)	169.6(3)	
O(2)-Al_O-O(4)×2	82.0(2)	81.5(2)	
O(3)-Al_O-O(4)×2	91.3(2)	91.4(2)	
O(4)-Al_O-O(4′)	93.3(2)	93.2(2)	
Al_O-O(1)-Al'_O	101.4(2)	102.1(3)	
Al_O-O(2)-M_T×3	123.6(2)	122.6(3)	
Al_O-O(2)-Al'_O×3	92.3(2)	93.7(2)	
Al_O-O(4)-Al'_O×3	103.7(2)	103.3(3)	

The lengths of bonds between aluminum and oxygens in the η^1-OH_2 groups are virtually identical (Table 3) at 1.961(4) Å for the Al_{13} and 1.962(6) Å for the $GaAl_{12}$ complex. This similarity is striking, given that rates of exchange of the η^1-OH_2 sites on the $GaAl_{12}$ are a factor of $\approx$5 times slower than in the Al_{13} molecule. The difference in lability of η^1-OH_2 sites on the Keggin-like molecule might be related to structural differences in the solvated $GaAl_{13}$ and Al_{13} molecules that are not present in the crystalline solid. Inclusion of the solvent waters in any computational model of these reactions may be essential.

4.3. Exchange of η^1-OH_2 Sites and Mineral Surfaces

Although the rates of exchange of η^1-OH_2 sites on the $GaAl_{12}$ molecule are considerably different than for the Al_{13} molecule, they are well within the range of values reported for other aluminum monomer and polyoxocation complexes (Table

Table 4. Rate coefficients and activation parameters for exchange of water molecules from the inner coordination sphere of Al(III) complexes to the bulk solution, as determined from ^{17}O-NMR. The estimated uncertainties for k_{ex}^{298} are reported as logarithms.

Species	k_{ex}^{298} (s^{-1})	$\pm\ln(\sigma)$	$\Delta H^{\ddagger}$ (kJ mol^{-1})	$\Delta S^{\ddagger}$ (JK^{-1} mol^{-1})	Source
Al^{3+}	1.29		84.7 (±3)	41.6 (±9)	Hugi-Cleary et al. (1985)
$Al(ssal)^{+}$	3000	0.08	37 (±3)	−54 (±9)	Sullivan et al. (1999)
$Al(sal)^{+}$	4900	0.07	35 (±3)	−57 (±11)	Sullivan et al. (1999)
$Al(mMal)^{+}$	660	0.18	66 (±1)	31 (±2)	Casey et al. (1998)
$Al(mMal)_2^{-}$	6900	0.02	55 (±3)	13 (±11)	Casey et al. (1998)
$Al(ox)^{+}$	109	0.13	68.9 (±2)	25.3 (±6.7)	Phillips et al. (1997b)
AlF^{2+}	111	0.14	79 (±3)	60 (±8)	Phillips et al. (1997a)
AlF_2^{+}	19,600	0.05	69 (±5)	70 (±17)	Phillips et al. (1997a)
$AlOH^{2+}$	31,000	0.25	36.4 (±5)	−36.4 (±15)	Nordin et al. (1998)
Al_{13}	1100	0.09	53 (±12)	−7 (±25)	Casey et al. (2000); Phillips et al. (2000)
$GaAl_{12}$	227	0.19	63 (±7)	29 (±21)	This paper

ox, oxalate; ssal, sulfosalicylate; sal, salicylate; mMal, methylmalonate; Al_{13}, $AlO_4Al_{12}(OH)_{24}(H_2O)_{12}^{7+}$(aq) complex; $GaAl_{12}$, $GaO_4Al_{12}(OH)_{24}(H_2O)_{12}^{7+}$(aq) complex.

4). The fact that rates for such structurally dissimilar molecules fall into a relatively narrow range is important because it supports the idea that the rates of exchange of η^1-OH_2 sites from the surface of a fully charged aluminum (hydr)oxide mineral also fall within this range of values $1 < k_{ex}^{298} < 10^4\ s^{-1}$ (Casey et al., 2000; Phillips et al., 2000). Two observations support this hypothesis. First, the charge density on the $GaAl_{12}$ and Al_{13} molecules is similar to that of a fully protonated oxide–mineral surface, 1 to 3 proton charges/nm^2 (e.g., Hiemstra et al., 1999; Nordin et al., 1999), so that electrostatic influences are probably comparable. Second, the mechanism of exchange of η^1-OH_2 sites in the Al_{13} and $GaAl_{12}$ molecules probably exhibits considerable dissociative character, by analogy with the mechanisms of exchange around Al^{3+}(aq) (Hugi-Cleary et al., 1985).

Although the range $1 < k_{ex}^{298} < 10^4\ s^{-1}$ is still quite large, it is much smaller than the total range of k_{ex}^{298} for different metals and complexes, which vary by well over a factor of 10^{15} (e.g., Richens, 1997). One could also narrow the range further to $10^2 < k_{ex}^{298} < 10^4\ s^{-1}$ by reasonably excluding Al^{3+}(aq) ion from the comparison because of its very high charge density.

4.4. Mechanisms of Exchange of μ_2-OH′ and μ_2-OH Sites

Any reasonable mechanism for exchange of the μ_2-OH sites probably involves water molecules as the nucleophile because there is no evidence for a strong pH dependence to the exchange rate. One possible mechanism involves partial dissociation of the Al–O bond in the bridge as a water molecule simultaneously coordinates to one of the two metals. The hydroxyl bridge exchanges with the water molecule to form a bridge that subsequently deprotonates to reform the hydroxyl bridge. The rate of this reaction is independent of pH because proton transfer from the bridging water molecule follows slow dissociation of the Al–OH bond, which is the rate-controlling step in the overall process.

An alternative mechanism was suggested to us by Dr. Pelmenschikov and Prof. Pettersson of Stockholm University that involves proton transfer to the hydroxyl from within the molecule, perhaps from an adjacent terminal η^1-OH_2 site, followed by exchange of the protonated bridge for a water molecule and back-transfer of the proton to the donor η^1-OH site, reforming the η^1-OH_2 site. This internal proton transfer mechanism has the advantage that one neutral water molecule exchanges for another, rather than for a hydroxyl ion, which must overcome electrostatic attraction to exchange. The corresponding quantum chemical calculations to test these mechanisms are currently in progress at Stockholm University.

Acknowledgments—The authors thank Marilyn Olmstead for discussing the X-ray crystal structures and for determining the structure of our starting material and Tom Swaddle for discussions about bonding and reactivity. Support for this research was from the U.S. National Science Foundation (NSF; grant EAR 98-14152) and from the U.S. Department of Energy (grant DE-FG03-96ER14629). The NMR spectrometers were purchased with grants from the National Institutes of Health (NIH 1S10-RR04795) and the NSF (BBS88-094739). We also acknowledge the Keck Foundation for support of the solid-state NMR center at the University of California, Davis.

Associate editor: G. Sposito

REFERENCES

Abragam A. (1961) *The Principles of Nuclear Magnetism.* Oxford University Press.

Amirbahman A., Gfeller M., and Furrer G. (2000) Kinetics and mechanism of ligand-promoted decomposition of the Keggin Al-13 polymer. *Geochim. Cosmochim. Acta* **64,** 911–919.

Allouche L., Gérardin C., Loiseau T., Férey G., and Taulelle F. (2000) Al_{30}: A giant aluminum polycation. *Angew. Chem. Int. Ed.* **39**, 511–514.

Bradley S. M., Kydd R. A., and Yamdagni R. (1990) Study of the hydrolysis of combined Al^{3+} and Ga^{3+} aqueous solutions: formation of an extremely stable $GaO_4Al_{12}(OH)_{24}(H_2O)_{12}^{7+}$ polyoxocation. *Magn. Res. Chem.* **28,** 746–750.

Bradley S. M., Kydd R. A., and Fyfe C. A. (1992) Characterization of the $GaO_4Al_{12}(OH)_{24}(H_2O)_{12}^{7+}$ polyoxocation by MAS NMR and infrared spectroscopies and powder X-ray diffraction. *Inorg. Chem.* **31,** 1181–1185.

Bradley S. M., Kydd R. A., and Howe R. F. (1993) The structure of Al-gels formed through base hydrolysis of Al^{3+} aqueous solutions. *J. Coll. Interf. Sci.* **159,** 405–422.

Casey W. H., Phillips B. L., Nordin J. P., and Sullivan D. J. (1998) The rates of exchange of water molecules from Al(III)-methylmalonate complexes: The effect of chelate ring size. *Geochim. Cosmochim. Acta* **62,** 2789–2797.

Casey W. H., Phillips B. L., Karlsson M., Nordin S., Nordin J. P., Sullivan D. J., and Neugebauer-Crawford S. (2000) Rates and mechanisms of oxygen exchanges between sites in the

$AlO_4Al_{12}(OH)_{24}(H_2O)_{12}^{7+}$(aq) complex and water: Implications for mineral surface chemistry. *Geochim. Cosmochim. Acta* **64,** 2951–2964.

Cossy C., Helm L., and Merbach A. E. (1988) Oxygen-17 nuclear magnetic resonance kinetic study of water exchange on the lanthanide(III) aqua ions. *Inorg. Chem.* **27,** 1973–1979.

Fu G., Nazar L. F., and Bain A. D. (1991) Aging processes of alumina sol gels—Characterization of new aluminum polyoxycations by Al-27 NMR spectroscopy. *Chem. Materials* **3,** 602–610.

Furrer G., Trusch B., Muller C. (1992a) The formation of the polynuclear Al_{13} under simulated natural conditions. *Geochim. Cosmochim. Acta* **56,** 3831–3838.

Furrer G., Ludwig C., and Schindler P. W. (1992b) On the chemistry of the Keggin Al-13 polymer. *J. Coll. Interf. Sci.* **149,** 56–67.

Furrer G., Gfeller M., and Wehrli B. (1999) On the chemistry of the Keggin Al-13 polymer-kinetics of proton-promoted dissolution. *Geochim. Cosmochim. Acta* **63,** 3069–3076.

Hiemstra T., Yong H., and Van Riemsdijk W. H. (1999) Interfacial charging behavior of aluminum (hydr)oxides. *Langmuir* **15,** 5942–5955.

Hugi-Cleary D., Helm L., and Merbach A. E. (1985) Variable temperature and variable pressure ^{17}O NMR study of water exchange of hexaquaaluminum(III). *Helv. Chim. Acta* **68,** 545–554.

Hugi-Cleary D., Helm L., and Merbach A. E. (1987) Water exchange on hexaaquagallium(III): High-pressure evidence for a dissociative interchange mechanism. *J. Am. Chem. Soc.* **109,** 4444–4450.

Johansson G. (1960) On the crystal structures of some basic aluminum salts. *Acta Chem. Scand.* **14,** 771–773.

Johansson G. (1962a) On the crystal structure of the basic aluminum sulfate $13 \cdot Al_2O_3 \cdot 6SO_3 \cdot xH_2O$. *Arkiv. Kemi.* **20,** 321–342.

Johansson G. (1962b) On the crystal structure of the basic aluminum selenate. *Arkiv. Kemi.* **20,** 305–319.

Johansson G., Lundgren G., Sillén L. G., and Söderquist R. (1960) On the crystal structure of a basic aluminum sulfate and the corresponding selenate. *Acta Chem. Scand.* **14,** 769–771.

Michot L. J., Montargès-Pelletier, Lartiges B. S., d'Espinose de la Caillerie B., and Briois V. (2000) Formation mechanism of the Ga_{13} Keggin ion: A combined EXAFS and NMR study. *J. Am. Chem. Soc.* **122,** 6048–6056.

Nordin J. P., Sullivan D. J., Phillips B. L., and Casey W. H. (1998) An ^{17}O-NMR study of the exchange of water on $AlOH(H_2O)_5^{2+}$(aq). *Inorg. Chem.* **37,** 4760–4763.

Nordin J. P., Sullivan D. J., Phillips B. L., and Casey W. H. (1999) Mechanisms for fluoride-promoted dissolution of bayerite [β-$Al(OH)_3$(s)] and boehmite [γ-AlOOH(s)]-^{19}F-NMR spectroscopy and aqueous surface chemistry. *Geochim. Cosmochim. Acta* **63,** 3513–3524.

Parker W. O'N., Jr., Millini R., and Kiricsi I. (1997) Metal substitution in Keggin-type tridecameric aluminum-oxo-hydroxy clusters. *Inorg. Chem.* **36,** 571–576.

Phillips B.L., Casey W. H., and Neugebauer-Crawford S. (1997a) Solvent exchange in $AlF_x(H_2O)_{6-x}^{3-x}$(aq) complexes: Ligand-directed labilization of water as an analogue for ligand-induced dissolution of oxide minerals. *Geochim. Cosmochim. Acta* **61,** 3041–3049.

Phillips B. L., Neugebauer-Crawford S., and Casey W. H. (1997b) Rate of water exchange between $Al(C_2O_4)(H_2O)_4^+$(aq) complexes and aqueous solution determined by ^{17}O-NMR spectroscopy. *Geochim. Cosmochim. Acta* **61,** 4965–4973.

Phillips B. L., Casey W. H., and Karlsson M. (2000) Bonding and reactivity at oxide mineral surfaces from model aqueous complexes. *Nature* **404,** 379–382.

Richens, D. T. (1997) *The Chemistry of Aqua Ions.* Wiley.

Rowsell J. and Nazar L. F. (2000) Speciation and thermal transformation in alumina sols: Structures of the polyhydroxyoxoaluminum cluster $[Al_{30}O_8(OH)_{56}(H_2O)_{26}]^{18+}$ and its Keggin moieté. *J. Am. Chem. Soc.* **122,** 3777–3778.

Springborg J. (1988) Hydroxo-bridged complexes of chromium(III), cobalt(III), rhodium(III) and iridium(III). *Adv. Inorg. Chem.* **32,** 55–169.

Sullivan D. J., Nordin J. P., Phillips B. L., and Casey W. H. (1999) The rates of water exchange in Al(III)-salicylate and Al(III)-sulfosalicylate complexes. *Geochim. Cosmochim. Acta* **63,** 1471–1480.

Swift T. J. and Connick R. E. (1962) NMR relaxation mechanisms of ^{17}O in aqueous solutions of paramagnetic cations and the lifetime of water molecules in the first coordination sphere. *J. Chem. Phys.* **37,** 307–320.

Thompson A. R., Kunwar A. C., Gutowsky H. S., and Oldfield E. (1987) Oxygen-17 and aluminum-27 nuclear magnetic resonance spectroscopic investigations of aluminum(III) hydrolysis products. *J. Chem. Soc. Dalton Trans.* **1987,** 2317–2322.